国立科博専報，(51), pp. 99–108 , 2016 年 3 月 28 日
Mem. Natl. Mus. Nat. Sci., Tokyo, (51), pp. 99–108, March 28, 2016

Kimuraite-(Y), a Layered Hydrous Carbonate of Calcium and Rare Earths, from Mikhailovsky District, Far East Russia

Ritsuro Miyawaki[1]*, Koichi Momma[1], Takashi Sano[1], Masako Shigeoka[1], Yukiyasu Tsutsumi[1], Sergei A. Kasatkin[2], Igor Chekryzhov[2] and Kazumi Yokoyama[1]

[1]Department of Geology and Paleontology, National Museum of Nature and Science, 4–1–1 Amakubo, Tsukuba, Ibaraki 305–0005, Japan
[2]Far East Geological Institute, Far Eastern Branch of the Russian Academy of Sciences 159, 100 let Vladivostok Pr, 690022, Russia
*E-mail: miyawaki@kahaku.go.jp

Abstract. Kimuraite-(Y) occurs in white veins of dark charcoal gray siliceous mudstone rich in Y (ca.1000–3000 ppm) in Abramovskoye, Mikhailovsky district, Primorye, Far East Russia. The mineral is associated with lanthanite-(Nd) and lokkaite-(Y). The white aggregate of minute crystals has a pearly to silky luster. An electron microprobe analysis (SEM-EDS) gave the following empirical formula: $Ca_{1.00}Y_{1.78}Ce_{0.01}Nd_{0.01}Gd_{0.01}Dy_{0.04}Ho_{0.03}Er_{0.06}Tm_{0.01}Yb_{0.04}Lu_{0.01}(CO_3)_4 \cdot 6H_2O$. The chondrite normalized lanthanoid pattern indicates the trend of Y-minerals, where it is rich in heavy rare earth elements. The orthorhombic unit cell parameters refined from powder XRD pattern are; a = 9.246(3), b = 23.974(8), c = 6.058(3) Å, and V = 1342.8(8) Å^3. The 5 strongest lines in the powder XRD pattern [d(Å) (I/I_0) hkl] are: 11.99 (96) 020; 5.99 (86) 040; 4.62 (100) 200; 3.76 (83) 051; and 2.08 (50) 431.
Key words: kimuraite-(Y), rare earth, Russia

Introduction

Kimuraite-(Y), ideally $CaY_2(CO_3)_4 \cdot 6H_2O$, was described in fissures in an alkali olivine basalt in Higashi-Matsuura district, Saga Prefecture, Japan, in association with lokkaite-(Y) and lanthanite-(Nd) (Nagashima *et al*., 1986). Later, the mineral was discovered in several other localities with different geological backgrounds. It was recognized as a secondary mineral on gadolinite-(Y) from a pegmatite in Ytterby, Sweden (Miyawaki, *et al*., 1993). Kimuraite-(Y) examined in the present mineralogical study was found in the Abramovskoye ore in the hydrothermal rare earth element (REE) mineralization in Cambrian carbonaceous shales, located at the periphery of the Voznesenskii ore region (Khankayskii massif, Primorskiy Kray), near the Pavlovsk brown coal deposit (Seredin, 1998). Kimuraite-(Y) occurs in white veins of dark charcoal gray siliceous mudstone, which was described as argillaceous rock of carbonaceous shale by Seredin (1998), in association with lanthanite-(Nd) and lokkaite-(Y) as reported in the previous study. The white aggregate of minute (less than few ten μm) flaky thin (less than 10μm) crystals shows a pearly to silky luster (Fig. 1).

Fig. 1. A photomicrograph of the white aggregates of minute flaky thin crystals of kimuraite-(Y). The field of view is 5.7 mm.

Chemistry

Chemical analyses of kimuraite-(Y) and the associated minerals were carried out with a JEOL JSM-6610/OXFORD X-Max SEM/EDS spectrometer using a lower beam current (15 kV, 0.6 nA, a beam diameter of 2 μm, and an approximate scan area of 4 μm^2) to avoid decomposing the hydrous carbonate minerals that can be damaged by the electron beam. The chemical composition of kimuraite-(Y), lanthanite-(Nd), and some associated calcium yttrium carbonate minerals are listed in Tables 1, 2, and 3, respectively. The empirical formulae for kimuraite-(Y) on the basis of 3 cations, 4 carbonate ions, and 6 water molecules *pfu* are:

$Ca_{1.00}Y_{1.78}Ce_{0.01}Nd_{0.01}Gd_{0.01}Dy_{0.04}Ho_{0.03}Er_{0.06}Tm_{0.01}Yb_{0.04}Lu_{0.01}(CO_3)_4 \cdot 6H_2O$ (1)

$Ca_{1.00}Y_{1.78}Pr_{0.01}Nd_{0.01}Sm_{0.01}Gd_{0.03}Dy_{0.04}Ho_{0.02}Er_{0.05}Tm_{0.01}Yb_{0.03}Lu_{0.01}(CO_3)_4 \cdot 6H_2O$ (2)

$Ca_{0.99}Y_{1.80}La_{0.02}Nd_{0.01}Sm_{0.01}Gd_{0.02}Dy_{0.04}Ho_{0.02}Er_{0.04}Yb_{0.03}Lu_{0.02}(CO_3)_4 \cdot 6H_2O$ (3)

$Ca_{1.00}Y_{1.80}La_{0.01}Nd_{0.01}Sm_{0.01}Gd_{0.02}Dy_{0.03}Ho_{0.02}Er_{0.04}Tm_{0.01}Yb_{0.03}Lu_{0.02}(CO_3)_4 \cdot 6H_2O$ (4)

$Ca_{0.98}Y_{1.82}La_{0.02}Nd_{0.01}Gd_{0.03}Tb_{0.01}Dy_{0.04}Ho_{0.01}Er_{0.04}Yb_{0.03}Lu_{0.01}(CO_3)_4 \cdot 6H_2O$ (5)

$Ca_{1.01}Y_{1.81}La_{0.01}Nd_{0.02}Gd_{0.02}Dy_{0.05}Ho_{0.01}Er_{0.04}Yb_{0.04}(CO_3)_4 \cdot 6H_2O$ (6)

Table 1. Chemical composition of kimuraite-(Y).

Constituent	Concentrations (wt.%)					
	1	2	3	4	5	6
CaO	9.41	9.33	8.99	8.45	8.17	7.63
Y_2O_3	33.69	33.79	33.20	30.90	30.31	27.43
La_2O_3	0.28	0.01	0.43	0.35	0.49	0.24
Ce_2O_3	0.00	0.00	0.01	0.01	0.10	0.00
Pr_2O_3	0.00	0.14	0.01	0.00	0.09	0.00
Nd_2O_3	0.28	0.35	0.24	0.24	0.28	0.40
Sm_2O_3	0.04	0.15	0.21	0.24	0.06	0.04
Gd_2O_3	0.35	0.76	0.59	0.45	0.70	0.59
Tb_2O_3	0.00	0.06	0.00	0.00	0.21	0.07
Dy_2O_3	1.15	1.13	1.12	0.73	1.10	1.30
Ho_2O_3	0.48	0.44	0.44	0.34	0.21	0.07
Er_2O_3	1.85	1.71	1.15	1.27	1.13	1.12
Tm_2O_3	0.36	0.27	0.00	0.15	0.00	0.00
Yb_2O_3	1.32	0.99	0.99	0.92	0.99	1.00
Lu_2O_3	0.27	0.25	0.50	0.46	0.20	0.00
CO_2	29.44	29.38	28.55	26.59	26.11	23.78
H_2O	18.08	18.04	17.53	16.33	16.03	14.60
total	97.00	96.79	93.95	87.43	86.19	78.27
	Atomic ratios on the basis of 3 cations, 4 carbonate ions and 6 water molecules *pfu*					
Ca	1.00	1.00	0.99	1.00	0.98	1.01
Y	1.78	1.78	1.80	1.80	1.82	1.81
La	0.01	0.00	0.02	0.01	0.02	0.01
Ce	0.00	0.00	0.00	0.00	0.00	0.00
Pr	0.00	0.01	0.00	0.00	0.00	0.00
Nd	0.01	0.01	0.01	0.01	0.01	0.02
Sm	0.00	0.01	0.01	0.01	0.00	0.00
Gd	0.01	0.03	0.02	0.02	0.03	0.02
Tb	0.00	0.00	0.00	0.00	0.01	0.00
Dy	0.04	0.04	0.04	0.03	0.04	0.05
Ho	0.03	0.02	0.02	0.02	0.01	0.00
Er	0.06	0.05	0.04	0.04	0.04	0.04
Tm	0.01	0.01	0.00	0.01	0.00	0.00
Yb	0.04	0.03	0.03	0.03	0.03	0.04
Lu	0.01	0.01	0.02	0.02	0.01	0.00
C	4	4	4	4	4	4
H	12	12	12	12	12	12

The hydrous carbonates of REE are often decomposed into other phases via in vacuo dehydration. Lanthanite-(Nd), $Nd_2(CO_3)_3 \cdot 8H_2O$, easily loses half of the crystallization water in vacuo to become $Nd_2(CO_3)_3 \cdot 4H_2O$, which corresponds to the Nd-analogue of calkinsite-(Ce). The chemical data of the present analysis suggested such a dehydration nature of lanthanite-(Nd) in vacuo. The empirical formula of lanthanite-(Nd) was calculated excluding the Si as an impurity and assuming full hydration of the crystal structure normalized to 2 rare earth (RE) cations, 3 carbonate ions, and 4 water molecules *pfu*:

$$Y_{0.11}La_{0.64}Pr_{0.17}Nd_{0.70}Sm_{0.24}Gd_{0.10}Dy_{0.04}(CO_3)_3 \cdot 4H_2O \quad (1)$$

$$Y_{0.11}La_{0.59}Pr_{0.16}Nd_{0.71}Sm_{0.25}Gd_{0.10}Tb_{0.01}Dy_{0.05}Yb_{0.01}(CO_3)_3 \cdot 4H_2O \quad (2)$$

The chondrite normalized lanthanoid patterns are given in Fig. 2.

Table 2. Chemical composition of lanthanite-(Nd).

Constituent	Concentrations (wt.%)	
	1	2
SiO_2	0.80	0.00
Y_2O_3	2.39	2.33
La_2O_3	20.44	18.07
Ce2O3	0.15	0.00
Pr_2O_3	5.52	5.11
Nd_2O_3	23.17	22.48
Sm_2O_3	8.26	8.13
Gd_2O_3	3.54	3.56
Tb_2O_3	0.00	0.30
Dy_2O_3	1.45	1.67
Ho_2O_3	0.00	0.00
Er_2O_3	0.00	0.39
Tm_2O_3	0.00	0.00
Yb_2O_3	0.00	0.15
Lu_2O_3	0.00	0.00
CO_2	25.97	24.81
H_2O	14.18	13.54
total	105.87	100.54
	Atomic ratios on the basis of 2 RE cations, 3 carbonate ions and 4 water molecules *pfu*	
Si	0.07	0.00
Y	0.11	0.11
La	0.64	0.59
Ce	0.00	0.00
Pr	0.17	0.16
Nd	0.70	0.71
Sm	0.24	0.25
Gd	0.10	0.10
Tb	0.00	0.01
Dy	0.04	0.05
Ho	0.00	0.00
Er	0.00	0.01
Tm	0.00	0.00
Yb	0.00	0.00
Lu	0.00	0.00
C	3	3
H	8	8

Two samples of the host rock were analyzed for their major and selected trace element compositions by X-ray fluorescence (XRF) and for their trace element compositions by acid-digested solution Inductively Coupled Plasma–Mass Spectrometry (ICP–MS). The rock samples were crushed into ~1 cm diameter grains, then, the grains were washed ultrasonically, twice in alcohol and twice in distilled water. The cleaned grains were dried for >12 hours in an oven at 110°C and then ground to powder in an agate mill. Before the major element analysis, ~0.4 g of the powder were weighed on a Metler Toledo dual balance system and heated at 1025°C for 4 hours in an electric muffle furnace to determine loss-on-ignition (LOI). After LOI determination, fused glass beads were prepared using a lithium tetra borate flux (10 : 1 dilution of sample). For the selected trace element analysis, ~4.0 g of powder were pressed into a pellet by a 12 ton force from a hydraulic press. The XRF analyses followed the method of Sano *et al*. (2011), except that a RIGAKU ZSX Primus II was used.

ICP–MS trace element concentrations were determined using a quadrupole Agilent 7700x following the procedures described by Chang *et al*. (2003), except that analyses of Li, Be, V, Zn, and Ga were also performed. Sample preparation involved digestion using an acid mixture comprised of HF–$HClO_4$–HNO_3, and the final dissolution was performed in 2% HNO_3 plus 0.1% HF spiked with ^{115}In and ^{209}Bi. These elements were added to standardize the signal for the ICP–MS measurements. The chemical compositions of the host rock samples are summarized in Table 4, together with the estimated values from the subsequent DTA-TG data.

The differential thermal-thermogravimetric (DTA-TG) curves were recorded on a RIGAKU

Table 3. Chemical compositions of associated calcium yttrium carbonate minerals.

Constituent	Concentrations (wt.%)											
	1	2	3	4	5	6	7	8	9	10	11	12
CaO	5.17	4.84	4.47	5.12	5.28	5.24	5.09	5.80	6.15	6.77	6.84	6.98
Y_2O_3	27.48	25.44	23.38	26.21	26.65	25.55	24.71	26.42	26.58	26.93	26.01	27.05
La_2O_3	0.36	0.21	0.33	0.24	0.32	0.33	0.32	0.20	0.31	0.28	0.15	0.22
Ce_2O_3	0.15	0.01	0.08	0.15	0.00	0.05	0.11	0.00	0.00	0.00	0.11	0.00
Pr_2O_3	0.15	0.30	0.00	0.43	0.20	0.34	0.18	0.28	0.23	0.13	0.26	0.13
Nd_2O_3	2.42	2.46	2.28	2.55	2.82	2.81	2.61	2.61	2.46	2.32	2.46	2.33
Sm_2O_3	2.49	2.94	2.52	3.01	2.86	2.63	2.93	2.28	2.36	2.75	2.65	2.44
Gd_2O_3	6.04	6.25	5.60	6.33	5.80	6.33	5.49	5.42	5.23	5.86	5.98	5.93
Tb_2O_3	0.80	0.50	0.44	0.52	0.14	0.87	0.30	0.57	0.47	0.54	0.55	0.59
Dy_2O_3	6.55	5.77	5.31	6.50	6.10	6.60	5.85	5.92	5.36	6.17	5.82	6.11
Ho_2O_3	1.00	0.68	1.00	0.53	0.96	0.56	1.05	0.90	0.62	0.57	0.87	0.84
Er_2O_3	2.16	2.46	2.46	2.32	2.58	2.14	2.86	2.44	2.36	2.19	2.58	2.35
Tm_2O_3	0.22	0.03	0.16	0.11	0.06	0.05	0.01	0.30	0.00	0.00	0.20	0.00
Yb_2O_3	1.45	1.07	0.71	1.47	1.02	1.15	0.89	0.85	0.86	0.64	0.81	0.67
CO_2	28.98	27.08	25.00	28.25	28.26	27.86	26.90	28.11	27.88	28.99	28.93	29.34
H_2O	11.94	11.15	10.29	11.58	11.47	11.28	10.87	11.00	10.61	10.75	10.66	10.78
total	97.36	91.18	84.03	95.32	94.52	93.79	90.17	93.10	91.48	94.89	94.88	95.75
	Atomic ratios on the basis of 1 Ca cation *pfu*											
Ca	1	1	1	1	1	1	1	1	1	1	1	1
Y	2.64	2.61	2.60	2.54	2.51	2.42	2.41	2.26	2.15	1.98	1.89	1.92
La	0.02	0.01	0.03	0.02	0.02	0.02	0.02	0.01	0.02	0.01	0.01	0.01
Ce	0.01	0.00	0.01	0.01	0.00	0.00	0.01	0.00	0.00	0.00	0.01	0.00
Pr	0.01	0.02	0.00	0.03	0.01	0.02	0.01	0.02	0.01	0.01	0.01	0.01
Nd	0.16	0.17	0.17	0.17	0.18	0.18	0.17	0.15	0.13	0.11	0.12	0.11
Sm	0.15	0.20	0.18	0.19	0.17	0.16	0.19	0.13	0.12	0.13	0.12	0.11
Gd	0.36	0.40	0.39	0.38	0.34	0.37	0.33	0.29	0.26	0.27	0.27	0.26
Tb	0.05	0.03	0.03	0.03	0.01	0.05	0.02	0.03	0.02	0.02	0.02	0.03
Dy	0.38	0.36	0.36	0.38	0.35	0.38	0.35	0.31	0.26	0.27	0.26	0.26
Ho	0.10	0.07	0.11	0.05	0.09	0.05	0.10	0.08	0.05	0.04	0.06	0.06
Er	0.12	0.15	0.16	0.13	0.14	0.12	0.16	0.12	0.11	0.09	0.11	0.10
Tm	0.01	0.00	0.01	0.01	0.00	0.00	0.00	0.02	0.00	0.00	0.01	0.00
Yb	0.08	0.06	0.05	0.08	0.05	0.06	0.05	0.04	0.04	0.03	0.03	0.03
ΣREE	4.10	4.09	4.08	4.02	3.88	3.85	3.82	3.45	3.18	2.97	2.93	2.90
C	7.14	7.13	7.13	7.03	6.82	6.78	6.73	6.18	5.78	5.46	5.39	5.36
H	14.38	14.34	14.34	14.08	13.52	13.40	13.29	11.80	10.74	9.88	9.70	9.61

Thermo plus 2 / TG-8120 thermal analyzer by heating 40 mg of each sample in a Pt cup from room temperature to 1150℃ at a rate of 10 degrees per minute (Fig. 3). The DTA curves showed endothermic peaks at around 155, 490, and 575℃. These endothermic reactions can be attributed to the dehydration of clay minerals such as kaolin-smectite in the rock sample. An exothermic peak at around 675℃ suggests combustion of carbonaceous materials, such as coal, peat, and bitumen including graphite, in the dark gray sample. One of the host rock samples, HR-A, gave an additional endothermic peak at around 770℃, which corresponds to the decarbonation of calcite (Rodriguez-Navarro, *et al*., 2009). The XRD reflections of calcite were confirmed with the powder XRD pattern of the host rock sample HR-A, for which the XRF analysis indicated considerable amounts of Ca (3.61 wt.% CaO; see Table 4). The amounts of H_2O, C, and CO_2 estimated from the weight loss accompanied with the 2 endothermic and 1 exothermic reactions are; 4.90, 3.44, and 2.12 wt.%, and 2.64, 4.51, and 0 wt.% for HR-A and HR-B, the 2 host rock samples, respectively. The individual values of total weight loss are comparable to the values of loss-on-ignition (LOI).

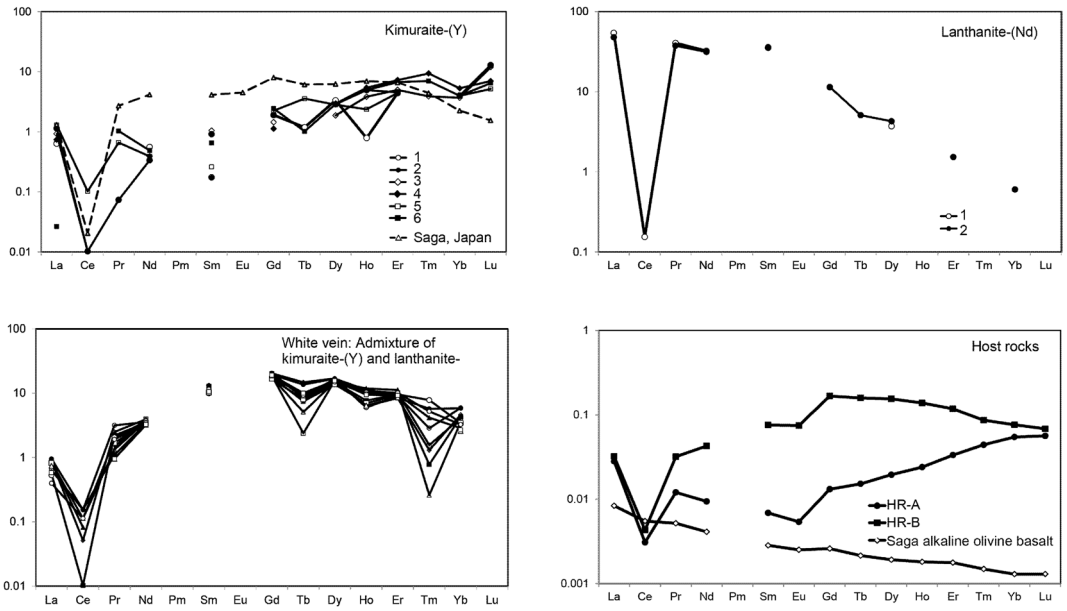

Fig. 2. Chondrite normalized lanthanoids patterns of kimuraite-(Y), lanthanite-(Nd), the mixture of kimuraite-(Y) and lanthanite-(Nd) and the host rock samples.

X-ray crystallography

The powder X-ray diffraction (XRD) patterns of kimuraite-(Y) and associated minerals in the white veins were obtained using a Gandolfi camera, 114.6 mm in diameter, employing Ni-filtered Cu *Kα* radiation. The exposures were carried out without vacuum deairing to avoid decomposition owing to the nature of kimuraite-(Y), therefore the dehydration occurred in vacuo. The data were recorded on an imaging plate (IP), were processed with a Fuji BAS-2500 bio-image analyzer using a computer program written by Nakamuta (1999), and were calibrated with an internal Si-standard reference material (NBS #640b). The unit cell parameters of the orthorhombic system were refined using a computer program by Toraya (1993); a = 9.246(3), b = 23.974(8), c = 6.058(3) Å, and V = 1342.8(8) Å^3. The XRD data of kimuraite-(Y) from Abramovskoye are shown in Table 5, with the XRD data of a mixture of kimuraite-(Y) and lokkaite-(Y) shown for comparison.

The XRD data of the host rocks were obtained with a conventional X-ray diffractometer (RIGAKU RINT2100; graphite monochromatized Cu *Kα* radiation, 20 kV 40 mA) in addition to the data from a Gandolfi camera. Quartz was determined to be the main constituent, and feldspar and some phyllosilicates having basal planes of 14.5 and 7.2 Å, which were possibly kaolin-smectite clays, were determined to be minor constituents. The XRD pattern of HR-A showed reflections of calcite as another minor constituent in the sample.

Some mineralogical and petrological aspects on the Russian kimuraite-(Y)

Kimuraite-(Y) from Mikhailovsky district, Russia shows several differences from the mineral from Saga, Japan, where is the type locality. The Russian specimen is colorless with smaller amounts of Nd (ca. 0.01 *apfu*), in comparison to the pale pinkish purple color of the type specimen with considerable amount of Nd (0.107 *apfu*). On the other hand, Y is more dominant (ca. 1.8 *apfu*) in the Russian kimuraite-(Y) than the type material (1.57 *apfu*). The dominance of Y-group REEs in the Russian kimuraite-(Y) is

Table 4. Chemical compositions of the host rock samples.

	HR-A	HR-B	Saga AOB*		HR-A	HR-B	Saga AOB*	HR-A	HR-B	Saga AOB*
Major constituent (wt.%) XRF					Minor elements (ppm) XRF			Minor elements (ppm) ICP-MS		
SiO_2	69.00	76.72	48.69	Li				26	26	7
TiO_2	0.79	0.87	1.75	Be				35	73	1
Al_2O_3	9.01	9.74	14.82	S	9	0	0			
Fe_2O_3	2.86	1.61	11.31	Sc				20	20	21
MnO	0.01	0.01	0.17	V	463	340	192	576	385	186
MgO	0.56	0.43	8.60	Cr	125	100	339			
CaO	3.61	0.35	8.77	Co	19	46	40	4	3	39
Na_2O	0.25	0.20	3.14	Ni	3402	2071	163	2367	1312	160
K_2O	2.00	3.18	1.60	Cu	66	98	56	76	102	46
P_2O_5	0.02	0.02	0.45	Zn	15041	8350	72	11407	5575	75
LOI	10.73	6.13	0.15	Ga				23	22	17
Total	98.84	99.26	99.45	As	25	25				
				Rb	65	107	39	70	104	33
Estimated concentrations (wt.%) TG				Sr	69	86	468	67	79	466
C	4.90	2.64		Y	898	2976	55	906	2616	52
CO_2	2.12	0.00		Zr	179	192	149	176	166	137
H_2O	3.44	4.51		Nb	29	61	34	17	14	28
sub total	10.46	7.15		Cs				4	5	0
				Ba	850	1224	519	856	1187	436
				La				91	104	27
				Ce	27	38	51	26	36	46
				Pr				14	37	6
				Nd				58	262	25
				Sm				14	150	6
				Eu				4	56	2
				Gd				35	450	7
				Tb				8	81	1
				Dy				66	525	7
				Ho				19	107	1
				Er				74	262	4
				Tm				15	29	1
				Yb				119	167	3
				Lu				19	23	0
				Hf				5	6	3
				Ta				1	1	1
				Tl				1	1	0
				Pb	61	59	2	58	51	3
				Th	13	15	4	10	12	4
				U				13	10	1

*Alkaline olivine basalt

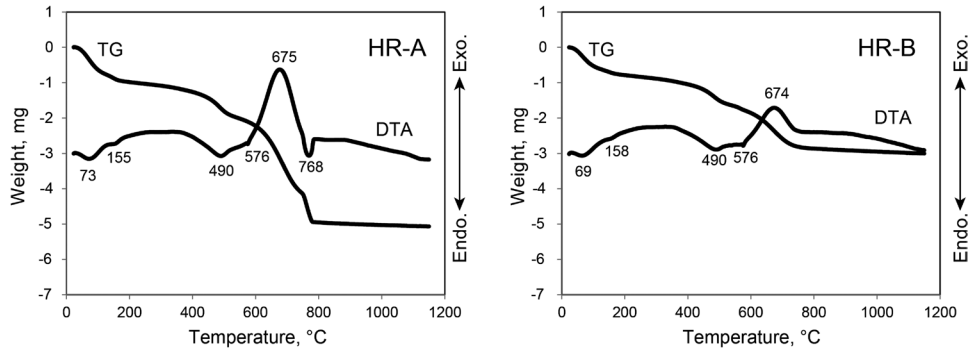

Fig. 3. DTA-TG curves of the host rock samples of kimuraite-(Y).

Table 5. XRD data of kimuraite-(Y).

Voznesenskii, Russia Kimuraite-(Y)			Voznesenskii, Russia Kimuraite-(Y)/ lokkaite-(Y)		Saga, Japan Kimuraite-(Y)					Saga, Japan lokkaite-(Y)				
I/I_0	$d_{obs.}$	$d_{calc.}$	I/I_0	$d_{obs.}$	h	k	l	I	d	h	k	l	I	d
			5	37.3										
			13	19.9						2	0	0	25	19.81
96	11.93	11.99	13	12.0	0	2	0	100	12.06					
			20	9.90						4	0	0	50	9.90
			6	8.92										
11	8.61	8.63			1	1	0	2	8.66					
			4	8.08										
			37	6.54						6	0	0	70	6.56
86	5.91	5.99			0	4	0	40	6.02					
		5.87	78	5.87	0	1	1	20	5.93	2	1	0	50	5.85
5	5.09	5.07	12	5.17	1	0	1	1	5.11	4	1	0	7	5.19
33	4.84	4.83	10	4.84	0	3	1	10	4.87					
100	4.62	4.62	100	4.62	2	0	0	10	4.64	0	0	2	55	4.62
			21	4.48						6	1	0	10	4.49
24	4.31	4.31	7	4.31	2	2	0	3	4.33					
12	3.99	4.00			0	6	0	20	4.01					
17	3.87	3.87	20	3.91	1	4	1	5	3.87	10	0	0	50	3.94
83	3.76	3.76	97	3.82	0	5	1	30	3.76	8	1	0	100	3.84
38	3.64	3.66	37	3.62	2	4	0	1	3.68	2	1	2	25	3.63
		3.63			2	1	1	6	3.64					
			17	3.44						4	1	2	7	3.45
45	3.34	3.34	15	3.34	2	3	1	7	3.35					
21*	3.14*	3.14	9*	3.15*	1	6	1	6	3.16					
			13	3.21						6	1	2	10	3.23
		3.03			0	0	2							
13	3.02	3.02	18	3.00	2	6	0	4	3.03					
		3.00			0	8	0	8	3.01	10	0	2	10	3.01
47	2.92	2.94	70	2.94	0	2	2	10	2.93	8	1	2	40	2.95
		2.92			2	5	1							
38	2.68	2.68	31	2.69	3	2	1	5	2.69					
10	2.58	2.58	13	2.59	1	8	1	5	2.59					
28	2.54	2.53	46	2.54	2	0	2	8	2.55	0	2	2	30	2.55
30	2.50	2.51			2	8	0	6	2.52					
		2.51			2	7	1							
		2.48	19	2.45	2	2	2	4	2.48	16	0	0	25	2.46
15	2.41	2.44	22	2.41	0	9	1	3	2.44	10	2	0	15	2.41
		2.41			0	6	2	4	2.42					
		2.40	6	2.37	0	10	0	6	2.41					
6	2.33	2.33			2	4	2	1	2.35					
9	2.31	2.31	10	2.30	4	0	0	1	2.32					
13	2.27	2.27			4	2	0	1	2.27					
6	2.22	2.20	7	2.24	1	7	2	1	2.23					
20	2.15	2.16	19	2.16	4	4	0	4	2.16	16	0	2	15	2.17
		2.16			2	9	1							
		2.15	24	2.14	4	1	1	4	2.15					
		2.15			3	1	2							
23	2.13	2.13	20	2.11	2	10	0	8	2.13					
		2.13			0	8	2							
50	2.09	2.08	18	2.09	4	3	1	7	2.09					
25	2.05	2.05	49	2.05	0	11	1	12	2.05	18	1	0	40	2.06
14	2.02	2.02	13	2.02	3	8	1	2	2.02					
		2.01			0	1	3	1	2.01					
		2.00			4	6	0							
24	1.968	1.969	35	1.972	4	5	1	4	1.972	18	0	2	10	1.979
		1.958			0	3	3	4	1.948					
15*	1.935*	1.935	6*	1.938*	2	8	2	4	1.934					

Table 5. continued

Voznesenskii, Russia Kimuraite-(Y)			Voznesenskii, Russia Kimuraite-(Y)/ lokkaite-(Y)		Saga, Japan Kimuraite-(Y)					Saga, Japan lokkaite-(Y)				
I/I_0	$d_{obs.}$	$d_{calc.}$	I/I_0	$d_{obs.}$	h	k	l	I	d	h	k	l	I	d
										16	2	0	15	1.913
28	1.875	1.880	36	1.876	0	10	2	9	1.881	8	3	0	20	1.882
		1.875			2	11	1	8	1.876					
		1.861			0	5	3	2	1.858					
		1.838			4	0	2	6	1.836					
38	1.826	1.830	27	1.836	4	8	0	6	1.832					
		1.816	9	1.808	4	2	2	4	1.818					
6	1.762	1.769	12	1.764	5	0	1	2	1.773					
		1.769			1	6	3	3	1.766					
		1.764			0	13	1							
		1.750			5	2	1	3	1.754					
13	1.739	1.739	13	1.738	0	7	3	4	1.741					
9	1.663		10	1.677										
7*	1.647*	1.648			2	13	1	2	1.648					
			7	1.602										
5	1.566		8	1.576										
5	1.544	1.545			0	15	1	2	1.547					
5	1.527		9	1.533										
		1.498	10	1.488	0	16	0	2	1.502					
		1.469	10	1.470	1	3	4	2	1.465					
9	1.466	1.468			6	3	1	2	1.469					
		1.468			0	4	4							
		1.466	9	1.453	2	15	1							
5	1.424		9	1.426										
5	1.401													
7	1.368	1.373	10	1.371	6	0	2	1	1.376					
		1.352			0	8	4	1	1.349					

* Estimaterd from data without the internal Si-standard, because of overlap by the reflections of Si.

suggested by the upward trend with abundances in heavy REEs, the typical trend for Y-dominant REE minerals, on the chondrite-normalized lanthanoid patterns (Fig. 2). The trend is not so significant for the type kimuraite-(Y) with abundant middle REE, e.g., Gd and Tb. On the contrary, lanthanite-(Nd) from Mikhailovsky district, Russia, shows a downward trend with abundances in light REEs, as well as lanthanite-(Nd) from other localities. All the patterns of the Russian specimens show a negative anomaly at the position of Ce (Fig. 2). This anomaly suggests some events under oxidizing conditions that led to the oxidation of Ce to separate the Ce^{4+} from the crystallizing system. The oxidizing conditions appear to have occurred at the source locality as well as in Higashi-Matsuura alkaline olivine basalt in Saga, Japan.

The difference in the REE composition has little effect on the unit cell parameters of kimuraite-(Y): a = 9.246(3), b = 23.974(8), c = 6.058(3) Å, and V = 1342.8(8) Å^3 [Mikhailovsky], a = 9.2545(8), b = 23.976(4), c = 6.0433(7) Å, and V = 1340.9(3) Å^3 [Saga]. It is worth noting that some minute fragments ($<100\,\mu$m) on the Gandolfi camera gave the XRD pattern of a mixture of kimuraite-(Y) and lokkaite-(Y). The XRD pattern indicates that the two REE carbonate minerals are closely associated with each other. An epitaxial overgrowth in the systematical stacking sequence is suspected in the fragments.

The host rock examined in the present study should correspond to the argillizated brecciated shale with adsorbed REEs and/or the stockwork of REE – carbonates (Seredin, 1998). Seredin (1998) suggested that the Abramovskoye ore occurrence and the Higashi-Matsuura alkaline

olivine basalt are characterized by a common geological feature that is related to the basaltic volcanism. The present chemical and crystallographic examinations on the host rock samples revealed that they are siliceous mudstone consisting of quartz as the main constituent mineral with minor kaolin-smectite clay minerals and K-feldspar with some carbonaceous materials and trace accessary minerals. The Mg- and Fe-poor host rock samples are not maffic, but are rather felsic. They showed no signature of basaltic volcanism origin.

The extraordinarily high REE concentration of the host rocks (Seredin, 1998) was confirmed by the present chemical analyses of the mudstone. The REE concentration is remarkably higher than those of the alkaline olivine basalt from Saga, Japan (Table 4). The alkaline olivine basalt indicated no Ce-anomaly, but a decreasing trend toward heavy REEs on the chondrite-normalized REE pattern (Fig. 2). The negative and positive Ce-anomalies in the rare earth carbonate minerals and weathered basalt, respectively, in Saga Prefecture suggest that the carbonate minerals are precipitation products after the separation of Ce^{4+}, which was oxidized during the weathering of the alkaline olivine basalt, from the source of the rare earth carbonate minerals (Watanabe *et al*., 2014). On the contrary, the host rock samples (HR-A and -B) showed chondrite-normalized REE patterns, which are comparable to those of the host rare earth carbonate minerals, having the Ce-anomaly and an increasing trend toward heavy REEs. The geological backgrounds of Mikhailovsky and Saga contrast with each other, whereas kimuraite-(Y) shows some commonalities in occurrence nature, e.g., the associated minerals and the negative Ce-anomaly, between the two localities across the Sea of Japan.

Acknowledgements

This joint investigation between the National Museum of Nature and Science, Tokyo, Japan and the Far East Geological Institute, Far Eastern Brach Russian Academy of Sciences, Vladivostok, Russia, was supported by the research project entitled "Research on the Earth's surface processes and biota in and near the Sea of Japan" of the National Museum of Nature and Science. The authors are grateful to Professor A. I. Khanchuk, Director, Academician of the Far East Geological Institute, Far Eastern Brach Russian Academy of Sciences, Vladivostok, Russia for his hospitable supports. We express our appreciation to Dr. S. Matsubara, curator emeritus of the National Museum of Nature and Science, for his comments and suggestions. Special thanks go to Dr. S. Uehara of Kyushu University and Mr. S. Iwano of the Mineral Friends of Fukuoka for their supports in the field research.

References

Chang, Q., T. Shibata, K. Shinotsuka, M. Yoshikawa & Y. Tatsumi, 2003. Precise determination of trace elements in geological standard rocks using inductively coupled plasma mass spectrometry. *Frontier Research on Earth Evolution* (IFREE Report for 2001–2002), **1**: 357–362.

Miyawaki, R., J. Kuriyama & I. Nakai, 1993. The redefinition of tengerite-(Y), $Y_2(CO_3)_3 \cdot 2–3H_2O$, and its crystal structure. *American Mineralogist*, **78**: 425–432.

Nagashima, K., R. Miyawaki, J. Takase, I. Nakai, K. Sakurai, S. Matsubara, A. Kato & S. Iwano, 1986. Kimuraite, $CaY_2(CO_3)_4 \cdot 6H_2O$, a new mineral from fissures in an alkali olivine basalt from Saga Prefecture, Japan, and new data on lokkaite. *American Mineralogist*, **71**: 1028–1033.

Nakamuta, Y, 1999. Precise analysis of a very small mineral by an X–ray diffraction method. *Journal of the Mineralogical Society of Japan*, **28**: 117–121 (in Japanese with English abstract).

Rodriguez-Navarro, C., E. Ruiz-Agudo, A. Luque, A. B. Rodriguez-Navarro & M. Ortega-Huertas, 2009. Thermal decomposition of calcite: Mechanisms of formation and textural evolution of CaO nanocrystals. *American Mineralogist*, **94**: 578–593.

Sano, T., T. Fukuoka & M. Ishimoto, 2011. Petrological constraints on magma evolution of the Fuji volcano: A case study for the 1707 Hoei eruption, in Studies on the Origin and Biodiversity in the Sagami Sea Fossa Magna Element and the Izu-Ogasawara (Bonin) Arc. *Memoirs of the National Museum of Nature and Science*, *Tokyo*, **47**: 471–496.

Seredin, V. V., 1998. Rare earth mineralization in Late Cenozoic explosion structures (Khanka massif, Primorskii Krai, Russia). *Geology of Ore Deposits,* **40**: 357–

371.
Toraya, H., 1993. The determination of unit–cell parameters from Bragg reflection data using a standard reference material but without a calibration curve. *Journal of Applied Crystallography*, **26**: 583–590.
Watanabe, Y., M. Hoshino & Y. Horiuchi, 2014. Genesis of the rare earth minerals in the Higashi Matsu-ura Basalt in the Saga Prefecture, Japan. *Rare Earth*s, **64**: 40–41 (in Japanese with English abstract).

極東ロシア産の木村石

宮脇律郎・門馬綱一・佐野貴司・堤　之恭・
Sergei A. Kasatkin・Igor Chekryzhov・横山一己

極東ロシア，プリモルスキー州産の木村石は，微細結晶が真珠から絹糸光沢を呈する白色集合体として，ロッカ石やネオジムランタン石を伴って，黒色ないしは暗褐色の泥岩中の白色脈として産する．母岩の泥岩は，微細な石英粒を主体とし，長石類，層状ケイ酸塩や石墨を含み，時に方解石を伴う．佐賀県産の原記載の木村石と類似の化学組成と結晶の単位格子を示すが，原記載の木村石に比べ，重希土の卓越が著しく，典型的なイットリウム鉱物の希土類パターンを持つ．原記載と同様に，セリウムとユウロピウムに負の異常が見られるが，母岩の泥岩は1000から3000 ppm程度の高いイットリウム濃度を示し，これまでに報告の無い特異的な成因が注目される．